Journal of Circuits, Systems, and Computers
Vol. 26, No. 11 (2017) 1750181 (30 pages)

DOI: 10.1142/S021812661750181X

World Scientific
www.worldscientific.com

An Efficient Method for Road Tracking from Satellite Images Using Hybrid Multi-Kernel Partial Least Square Analysis and Particle Filter*

K. Madhan Kumar†
Department of Electronics and Communication Engineering,
PET Engineering College, Vallioor
madhankumar0879@gmail.com

A. Velayudham
Department of Information Technology,
Cape Institute of Technology,
Levengipuram – 627114
Tirunelveli District

R. Kanthavel
Rajalakshmi Institute of Technology, Chennai

Received 23 December 2015
Accepted 6 March 2017
Published

The Road extraction from the remotely sensed imagery is highly realistic for the quick road updating in the Geographic Information System (GIS) data collection. The particle filter (PF) was earlier employed to track the road maps in satellite images. In our previous work, we have introduced an efficient Gauss–Hermite Kalman Filter with Locally Excitatory Globally Inhibitory Oscillator Networks (GHKF–LEGION)-based road extraction, even though it does not properly extract the road from the complex region. In order to recover the track of the road beyond obstacles, in this work, we proposed a novel hybrid multi-kernel partial least squares (PLS) with PF approach. Here, at first, we estimate the initial leader point of the road employing the K-means clustering technique. Subsequently, the PF traces a road till a stopping benchmark is satisfied. Thereafter, without finishing the process, the outcomes are furnished to the hybrid kernel PLS technique which attempts to locate the continuance of the road after several potential road blocks or to locate the entire feasible road branches which are on the other side of the road junction. The outcomes are offered for five satellite images. The experimental results show our proposed road tracking method is better compared to other existing works.

AQ: Please provide keywords.

Keywords:

*This paper was recommended by Regional Editor Piero Malcovati.
†Corresponding author.

1. Introduction

There is no second opinion on the fact that, nowadays, a network of roads has emerged as an indispensable medium of transport and it constitutes one of the four pillars of human civilization. With the result, it has become highly essential to preserve and restore roads to maintain the transport network duly linked. The roads habitually take the shape of dark lines when observed from the satellite images which are by and largely accurate in the rural and suburban scenarios.[1] Of late, the road extraction from the satellite imagery has become the cynosure of attention and attraction among the investigating community. It is especially deployed in the city planning, cartography and to renovate the earlier identified roads in the Geographic Information Systems (GIS) settings.[2] The urban road mapping from the high spatial resolution images constitutes an invaluable as they facilitate the distinction of urban characteristics, though they bring in their train a host of novel issues as a number of the urban characteristics may be deemed as part and parcel of noise.[3] Habitually, the semiautomatic techniques function either as road followers identical to the techniques proposed in Refs. 5 and 6, or as the concurrent curve-fitting trackers such as the techniques based on active contour models,[4] piecewise parabola fitting,[7] and dynamic programming (DP) optimization.[8] Even then, the automated methods generally need the skilled integration of the contextual data and *a priori* knowledge in the road extraction process.[3,9] Several novel techniques were brought to spotlight intended for the assessment of the tracking of the road during the course of the last decade.[10,11] It is very essential for several applications to update and revise the road network data.

AQ: Please check sentence. Is something missing after invaluable?

A homogeneity characteristic of the pixel was employed to extort the road feature from the satellite images.[12] The gradient operation-based[13] road skeletal formation was appropriate for the rural roads. The road extraction by level segmentation and morphological function[14] were performed on high-resolution satellite images. Nevertheless, the perfect automation of the road extraction procedures continues to be a hard nut to crack and is evading solutions with a logical degree of success (accuracy) over a titanic set of images of diverse types of urban and suburban scenarios. In this regard, one of the significant classes of road-tracking (RT) techniques is dependent on the probabilistic modeling of related data and Bayesian evaluation method, where statistical models are employed to represent the distinctiveness of the road features. As a rule, the captioned methods encompass two phases such as the prediction phase and update phase. The technique dependent on the extended Kalman filter (EKF) represents one of the vital techniques in this class, which was kickstarted for the road map extraction in Ref. 15 and thereafter was again renovated in Refs. 3 and 6. The particle filters (PFs) are usually employed for the nonlinear filtering. The techniques based on the PF were employed in Refs. 16 and 17 to trace a single road path initiated by a specified seed at the commencement of the road. One of the glaring defects in the prior works linked with the above-cited class of road extraction

techniques[3,6,15–17] lies on the restricted processing area on the image. The corresponding techniques utilize either EKF or PF, begin tracing a road from a specified seed point on the road, and generally stop when they arrive at a stern occlusion, an intersection, or even remarkable change in the road direction.

In the past few years, a feast of novel techniques has been given the green signal to successfully address the recognition of roads from the satellite images. Standing out amongst them are the knowledge-based techniques, mathematical morphology,[18–20] snakes,[3,21] classification,[22] differential geometry,[23] region competition,[24] active testing,[25] perceptual grouping[26] and the DP.[27] Further, the representative work under the Bayesian structure may be broadly categorized into two types: (a) the state evaluation for the linear and Gaussian model employing the Kalman filter and its variants like the fragrance-free Kalman filter and comprehensive Kalman filter, and (b) the state evaluation for the nonlinear and non-Gaussian challenge by deploying the sequential Monte Carlo approaches[28] otherwise termed as the condensation filter,[29] bootstrap filter[30] and the PF.[31,32] The sterling merits of the sequential Monte Carlo approaches PF involve the scaling down of the sampling patches in the course of the tracking and its incredible skills of effectively addressing multi-modal distribution created by cluttered scenario. The advancement or augmentation of the semiautomatic methods is highly essential to facilitate the quick, reliable and accurate furnishing of the data for the GIS techniques like the complete, or just approximately complete, mechanized procedures which have not failed to turn the corner and become sufficiently mature.[33]

Global AQ: Please check we have changed k-clusters, k-means to K-clusters, K-mean & U_k to U_K; W_k to W_k, W^i_k, W^j_k to W^i_k, W^j_k

2. Related Works

It is worth mentioning that a feast of relevant investigations have been carried out by the disinterested investigators with the intention of the extraction of satellite images. Table 1 illustrates the evaluation of a few modern associated works regarding the extortion of the satellite images. A road tracker, based on angular texture signature, was kickstarted by Shen *et al.*[34] in accordance with skills acquired regarding the roads on high-resolution imagery. The existing stipulations implied that the technique would meet with failure on a road cast by incredibly shadow and occlusion in complicated scenarios. It was only capable of tracking the long ribbon roads on grayscale imagery, requiring excessive evaluation time. The outcomes were exhibited by means of a single high-resolution satellite image sample. The mean-shift clustering technique was effectively employed within the hue–saturation–intensity space. The conditional morphological approaches were utilized to considerably perk up the segmentation outcomes in Ref. 35. A model and a strategy dependent on the multiscale recognition of the roads in juxtaposition with the geometry-constrained edge extraction making use of the snakes were offered in Ref. 36. Outcomes were exhibited for three sample images, and the related technique was invariably meant for the rural areas. A host of coordinating snakes,[37] which were competent to split, merge and

Table 1. Summary of related methods in road extraction.

Methods	Feature	Number of samples used as test case
Road tracker, angular texture signature[34]	Intensity and edge detection	2–4
Mean shift clustering[35]	Histogram of HSI image	1–8
Snakes[36]	Intensity gradient	3
SVM[38]	Intensity, edge gradient, edge length, width	3–6
Region competition[28]	Intensity	4
Binarization, optimization using Markov random field[39]	Mean radiance value	5
Perceptual grouping algorithm[41]	Intensity, edge	2–3
Toe finding algorithm[42]	Intensity, shape	3–4
Fast linear feature detector algorithm[11]	Intensity, linear features	2
Multi-scale geometric analysis of detector responses[12]	Shape, road point	1
DP algorithm[43]	Direction, radiometric information	2
Unscented kalman filter (UKF) and gauss–hermite kalman filter (GHKF) (previous work)[45]	Shapes, color, intensity	3
Locally excitatory globally inhibitory oscillator networks (LEGION) and GHKF (previous work)[46]	Shapes, color, intensity	3
Ours proposed work	Shapes, color, intensity	5

disappear as and when needed were employed to extort the detached road networks and the enclosed areas. The energy functional consisted of the gradient vector flow evaluated as a diffusion of the gradient vectors of a gray level or binary edge map attained from the image.

A Lion's share of the modern road extraction approaches for multi-spectral imagery invariably depends on a mechanized and consistent classification of road surfaces. However, it is unfortunate that the classification precision of roads fares poorly irrespective of whether a supervised or unsupervised classification technique is used. The cardinal roadblock is related to the excessive misclassification between the roads and the spectrally analogous objects including the parking lots, buildings, crop fields, to name a few. Song and Civco[38] effectively employed two shape measures such as the smoothness and compactness to considerably decrease the misclassification between roads and other spectrally identical objects in a support vector machine (SVM) classifier. Further, Amo *et al.*[28] were instrumental in launching the road extraction employing the region competition technique. An initial simple model was distorted by means of the region growing algorithms to achieve a coarse road approximation. This model was improved by regional competition. In Ref. 39, Negri *et al.* convincingly discussed explained the junction-aware extraction and regularization of the urban road networks in high-resolution synthetic aperture radar (SAR) images, although the technique met with a waterloo in its role as the road detector.

AQ: Please approve edit.

Sahar and Alireza[40] amazingly launched a significant road tracing technique making use of the comprehensive Kalman filter and a special PF module. These modules, employing the clustering techniques, were capable of overcoming all the hindrances on the road and track all the road branches at a junction. In fact, all road segments in a linked road network were tracked by means of a single seed point. Nevertheless, the efficiency of the technique solely depended on the parameters of the module. A novel technique was green-signaled and implemented by Paolo Gamba *et al.*[41] for detecting the urban road networks from the high-resolution optical/SAR images. The perceptual grouping technique was employed to recoup the local flaws and also to rebuild the normal roads in the images. The vital constraint of the innovative technique was the substandard precision as the overall precision range was a mere 45.48%.

AQ: Please check.

An automatic technique for extorting road from the aerial imagery was brought to the spotlight by Hu *et al.*[42] In view of the excessive extortion, the tracking of road footprints was adversely affected. With an eye on finding a solution to this hassle, an innovative method was envisaged by Shao *et al.*[11] for designing a quick and efficient technique for identifying the ridge- or ribbon-like linear features from the remote sensing imagery. The aerial images were deployed to verify the efficiency of the technique in the extortion of the roads. An innovative road network grouping technique was coined by He *et al.*[12] for the SAR images by employing the multi-scale geometric assessment of the detector feedbacks. The roadmap of the algorithm consisted of three stages. (1) the extraction of guidance segments, (2) segment labeling and (3) the grouping of the road guidance segments. Further, a well-orchestrated semiautomatic technique for the 3D road extraction in rural areas employing the stereoscopic aerial images was envisaged by Dal Poz *et al.*[43] The appealing test outcomes illustrated without an iota of doubt that the innovative approach was skilled enough to usher in amazingly accurate road centerlines. A novel technique was flagged off by Miao *et al.*[44] to extort the road centerline from the high-resolution imagery depending on the shape features and the multi-variate adaptive regression splines (MARS). The cardinal constraint of captivating technique was that the thresholds in the technique had to be manually evaluated and that it was not the appropriate candidate for the low-resolution images.

Considering the above challenges, an efficient approach is urgently needed to improve the road extraction limitations. In this paper, we have proposed a road extraction approach to extract road region from the satellite images. Then, the performance of the procedure is tested on five different satellite images. The rest of the paper is organized as follows. Introduction is explained in Secs. 1 and 2 explains the related works. The design strategy of proposed method is explained in Sec. 3 and justification of the different stages for RT process is explained in Sec. 4. Result and discussion are provided in Sec. 5, finally, the conclusion is summed up in Sec. 6.

AQ: Please approve edit.

3. Design Strategy and Proposed Methodology for RT

3.1. *Road design*

The grave challenges in the design of an automated road network extraction mechanism employing the remotely sensed imagery lie in the fact that the image traits of road feature change depending on the sensor type, spectral and spatial resolution, ground traits and so on. Even with respect to an image obtained over a specific urban region, diverse segments of the road network expose diverse features. In the actual world, a road network is so complicated that it is very difficult to model by means of a mathematical formulation or a theoretical structural model. The existence of other objects such as the buildings and trees emits shadows to occlude road features, thereby making the extraction procedure further complex.

The human perceptual methods of identifying a road include[48] the extraction of the geometric, radiometric and topological features of an image. The human beings habitually identify a road deploying initially its geometric features, creating a road to be an extensive and stretched out feature with identical width and analog radiometric variation all through its path. Though the spectral features of a road fluctuate within an image, its physical appearance tends to exist with the elongated and incessant traits. The human beings blend these critical clues to locate a foreground road object from the background layer. This phenomenon has motivated us to design a generic structure which integrates the appropriate processing modules essential for the extortion of various categories of features available in the road objects from satellite scenes. In the configuration of the RT issue, as in Ref. 2, we employ a 4D state vector as follows:

$$U_K = [R_k \; C_k \; \Phi_k \; \overline{\Phi_k}] \,,$$

where R_k is row of the center of the road, C_k is column of the center of the road, Φ_k is road direction and $\overline{\Phi}_k$ is change in road direction.

These roads are endowed with a characteristically distinct spectral signature locally and universally in relation to the background layer such as the vegetation, soil, waterways and the synthetic structures, to name a few. The corresponding road framework is fruitfully employed in our technique.

3.2. *Design of PF*

The PF was kickstarted in 1993 by Gordon as the bootstrap filter for evaluation of the nonlinear and non-Gaussian states.[47] In the PF, the state at each time instant is characterized by sample-based probability density function (PDF). The sequential Monte Carlo technique with significant sampling is elegantly employed for the evaluation of the nonlinear and non-Gaussian state. The underlying motive of the PF is to evaluate the state of the system by means of the weighted mean of particles available in the vicinity of state space. It represents a recursive procedure

where the prior state is revised by means of the online measurements (weights) to ascertain the subsequent state evaluation. When the evaluation of a subsequent state is finished, it functions as prior for the succeeding state evaluation. The weights in the PF represent probability measure between the posterior probability density and reference prior probability density. Even though the PF concept is voluminously discussed in the literature, we have given an introduction of the PF concept with a concise description solely for the purpose of the conclusion of the research document.

For the evaluation of the subsequent state of the mechanism, the target model is shortlisted which demarcate various features such as the motion, scaling, rotation factor for the target. In accordance with Eq. (1), the target model is configured.

$$U_K = H_{K-1}(U_{K-1}, M_{K-1})\,. \tag{1}$$

Here, $H_{K-1} : R^m \times R^n \to R^m$ is the nonlinear function of target state with a dimension of m; $M_{k-1} \in R^n$ is white noise sequence of dimension n with zero mean (known PDF) represents the uncertainty in state prediction. Also, online discrete measurement $V_K \in R^v, K \geq 1$ up to current time K are made according to measurement Eq. (2)

$$V_K = G_K(U_K, Z_K)\,, \tag{2}$$

where $G_K : R^k \times R^q \to R^v$ is a nonlinear function, Z_K is zero mean, white noise sequence (PDF known) representing an error in measurements. Recursive process of PF consists of two steps as (i) prediction, (ii) updating from the given online measurement sequences $V_K = \{V_i : i = 1, 2, \ldots, K\}$. In prediction step, prior PDF at time instant K is determined as

$$P(U_K|V_{K-1}) = \int P(U_K|U_{K-1})P(U_{K-1}|V_{K-1})dU_{K-1}\,, \tag{3}$$

where in Eq. (3) prior PDF is obtained using system model Eq. (1) and initial PDF at time $K-1$, i.e., $P(U_{K-1}|V_{K-1})$. In update step, the problem is to estimate the posterior density $P(U_{0:K}|V_{1:K})$ using the Bayes rules as defined in Eq. (4) at every time-step is given in the prior PDF $P(U_0|V_1) \equiv P(U_1)$ functional form of state (H) and measurement (G) up to that time instant. The same can be expressed as

$$P(U_K|V_K) = \frac{P(V_K|V_{0:K})P(V_K|V_{K-1})}{P(V_K|V_{K-1})}\,. \tag{4}$$

In PF, Eqs. (3) and (4) form the recursive process for state estimation. Considering the tracking problem N random samples $[U_1^{(i)}]_{i=1,2,\ldots,N}$ are taken from initial given PDF $P(U_1)$. These samples are passed through system state model equation (1) in order to obtain predicted N particles. The predicted particles are assigned normalized weights using Eq. (5).

AQ: Please check the edit.

$$W_j = \frac{P(V_K|U_K(j))}{\sum_{j=1}^{N} P(V_K|U_K(j))}, \quad \text{where } j = 1, 2, \ldots, N. \tag{5}$$

AQ: Please check edit.

Because the target dynamics are assumed to be Markov chain, posterior can be represented as

$$P(U_K|V_{1:K}) \approx \sum_{j=1}^{N} W_K^j \, \delta(U_K - U_K^i), \tag{6}$$

where $\delta(\bullet)$ represents the Dirac delta function on account of the deterministic nature of Eq. (1) for the specified value of U_{K-1} and W_{K-1}. At last, the revised particles function as the prior for the succeeding state prior particles and this recursive procedure goes on until the last state forecast and revision. If the dimension of the particle is enhanced, the precision of the tracking gets perked up, though it entails additional processing power. In actual practice, only a restricted number of particles are used for the tracking application. Further, after little state evaluation, the number of particles with negligible weights goes up and the upkeep of these tiny particles whose contribution to evaluation is trivial need added computational power. Hence, the resampling is initiated on revised particles so as to ignore the particles having insignificant weights.[8] In the resampling process, new samples $[*U_K^i]_{i=1,2,\ldots,N}$ are created by resampling N times from the evaluated PDF $P(U_K|V_{1:K})$ in order that for any $j \Pr[*U_K^i = U_K^j]_{i=1,2,\ldots,N} = W_K^j$. The pseudo-code of the PF is furnished in Table 2.

Table 2. Pseudo-code for PF.

Input:
Satellite image
Parameters of PFs
1. For $j = 1 : N$
2. At time $K = 1$
3. Randomly sample PDF $P(U_{K-1}\|V_{1:K-1})$ for selecting N Samples $[U_{K-1}^{(i)}]_{i=1,2,\ldots,N}$
4. Assign weight to particle as per Eq. (5)
5. Calculate the sum of weight $W_{\text{sum}} = \sum_{i=1}^{N} W_i$
6. Normalize the weight for particles.
7. Resample: generate new samples $[U_K^{(i)}, W_K^{(i)}]_{i=1,2,\ldots,N}$ based upon W_K^i after resampling of N updated particles so that $\Pr[*U_K^{(i)} = U_K^j]_{i=1,2,\ldots,N} = W_K^j$
8. Estimate the state by $U_K = \frac{1}{N} \sum_{i=1}^{N} X_k^i$
9. $k+1 \leftarrow k, j+1 \leftarrow j$
10. Go to Step 3
Output:
Tracked road

3.3. *Design of partial least squares analysis*

Partial least squares (PLS) analysis[49] represents a statistical technique for designing the relations between sets of variables through certain latent quantities. In the PLS evaluation, the observed data is deemed to be created by a procedure motivated by an insignificant number of latent variables. Let $U \in R^m$ represent an m-dimensional space of variable and $V \in R^n$ symbolize an n-dimensional space of other variables. With N observed samples from each space $u \in U$ and $v \in V$ from the two block of variables, $U \in R^{N\times m}$ and $V \in R^{N\times n}$, PLS techniques locate new spaces where large deviations of the observed samples can be maintained, and the skilled latent variables from the two blocks are highly associated vis-à-vis those in the original spaces,

$$\begin{aligned} U &= XM^T + I\,, \\ V &= YN^T + J\,, \end{aligned} \tag{7}$$

where

$X \in R^{N\times p}, Y \in R^{N\times P} \rightarrow$ factor (score component) matrices,

$M \in R^{m\times p}, N \in R^{n\times p} \rightarrow$ loading matrices,

$I \in R^{N\times m}, J \in R^{N\times n} \rightarrow$ error terms,

To decompose U and V by Eq. (1), PLS algorithms first compute the weight vectors a_1 and b_1 such that most variations in U and V can be retained by $x_1 = Ua_1$ and $y_1 = Vb_1$.

$$\begin{aligned} &\max_{a_1} |\mathrm{Var}(x_1)\,, \\ &\max_{b_1} \mathrm{Var}(y_1)\,, \end{aligned} \tag{8}$$

where

x_1 and y_1 are first columns of X and $Y, \mathrm{Var}(\bullet)$ is Variance.

Meanwhile, PLS analysis also requires x_1 besting explaining y_1

$$\max_{a_1,b_1} \mathrm{Var}(x_1, y_1)\,, \tag{9}$$

where $\rho(x_1, y_1) = \mathrm{Cov}(x_1, y_1)/\sqrt{\mathrm{Var}(x_1)\mathrm{Var}(y_1)}$ defines the correlation coefficient between x_1 and y_1 and $\mathrm{Cov}(x_1, y_1) = x_1 y_1/N$ denotes the sample covariance between x_1 and y_1. Combining Eqs. (2) and (3), PLS analysis maximizes the covariance between x_1 and y_1 in the first step

$$\max_{a_1,b_1} \mathrm{Cov}(x_1, y_1) = \max_{a_1,b_1} \sqrt{\mathrm{Var}(x_1)\mathrm{Var}(y_1)}\rho(x_1, y_1)\,. \tag{10}$$

Therefore, a_1 and b_1 can be computed by solving the following optimization problem:

$$\begin{aligned} &\max\langle Ua_1, Vb_1\rangle\,, \\ &st\ a_1^T a_1 = 1, \quad b_1^T b_1 = 1\,, \end{aligned} \tag{11}$$

where $\langle Ua_1, Vb_1 \rangle$ denotes the inter-product of Ua_1 and Vb_1. The optimal weight vector a_1 for above optimization problem is the first eigenvector of the following eigenvector problem[19]:

$$U^T V V^T U a_1 = \lambda a_1 . \tag{12}$$

Similarly, b_1 can be obtained by solving another eigenvalue problem

$$V^T U U^T V b_1 = \lambda b_1 . \tag{13}$$

After the first step, the PLS method iteratively computes other weight vectors. When a_1 and b_1 are available, the score vectors can be computed by $x_1 = Ua_1$, $y_1 = Vb_1$, and loadings (first columns of M and N) can be computed by $m_1 = \frac{U^T x_1}{x_1^T x_1}$ and $n_1 = \frac{V^T y_1}{y_1^T y_1}$, respectively. The data matrices U and V are the deflated by subtracting their rank- one approximation.

$$\begin{aligned} U &\leftarrow U - x_1 m_1^T , \\ V &\leftarrow V - y_1 n_1^T . \end{aligned} \tag{14}$$

Then new U and V are used to compute a_2 and b_2 based on Eqs. (12) and (13). This process is repeated until the residuals are small enough or a predefined number of weight vectors $a_1, a_2, \ldots, a_p$ and $b_1, b_2, \ldots, b_p$ are obtained.

4. Justification of the Different Stages for RT Process

The basic idea of our work is to track the road in satellite image using PLS–PF. The RT algorithm is based on probabilistic modeling of associated data and Bayesian estimation techniques. Basically, RT methods consist of two stages such as prediction stage and update stage. In our work, PF is used in combination with PLS to recognize and trace various connected road paths and to avoid obstacles under various conditions. The PF component is responsible for tracking axis coordinates of a road until it comes to severe obstacles or an intersection. Then, the PLS module takes the control of the algorithm and regains track of the road or possibly road branches on the other side of a junction or obstacles. Our work consists of two important stages. (i) K-means clustering-based seed point selection, and (ii) measurement model for object tracking. The overall structure of proposed RT is given in Fig. 1.

4.1. *K-means clustering-based seed point selection*

The basic idea of seed point selection is to give the root to tracking road in satellite image which is the initial step to tracking process. In order to apply PF to trace a road in satellite images, we need to consider of the road median on images as a random process. The processing system PF can start its operation from a seed point

Fig. 1. Five input images.

(initial point) on the road. This initial point can be provided by a human operator or through automatic approach, this selection is very important to the RT results. In our work, at first, we manually generated reference road model R_1 with is in the form of $m \times n$ which is helpful for seed point selection. Based on R_1, we calculate the initial seed point. After that, we split the satellite image into a number of $m \times n$ the matrix which matrix are converted into a vector format that means each matrix values are arranged into row format. For example, $n = 7, m = 7$ means we select the reference road model R_1 is in the form of 7×7 a matrix. After that we split all the pixel present in the satellite image is converted into 7×7 the matrix. Finally, we arrange all matrix into vector format, which vector having the 49 block of vectors. In this vector, we apply the K-means clustering algorithm for the selection of the initial point of the road which has traced the road path then calculates the minimum distance based on the following objective function.

$$J = \sum_{i=1}^{k} \sum_{j=1}^{n} \|x_j^{(i)} - c_i\|^2 , \tag{15}$$

where $\|x_j^{(i)} - c_i\|^2$ is a chosen distance measure between a data point $x_j^{(i)}$. c_j is the cluster center.

For K-means clustering process, at first, we select the k initial (in this technique $k = 10, 15$ and 20) are randomly generated within satellite image. K-clusters are generated by associating every observation with the nearest mean. The centroid of each of the k-clusters becomes the new mean. Which process is repeated until convergence has been reached. Finally, we obtain N number of centroid and N number of clusters. After that reference model R_1 is matched with each cluster, one less

Table 3. Pseudo-code for seed point selection.

Input
Satellite image
Parameters of K-means algorithm
Output
Initial seed points in road R_2
start
Get the input image S_{im} from the system
Randomly select one reference profile R_1 which is in the form of $n \times m$ matrix
Based on the reference point R_1 we create the grid structure of input image S_{im}
Arrange each grid pixel value into row format based on the grid structure
Repeat
Apply K-means algorithm for initial point selection
Calculate the minimum distance using Eq. (15)
For K-means process
{
randomly generated k value from the satellite image
K-clusters are generated by associating every observation with the nearest mean.
The centroid of each of the K-clusters becomes the new mean
}
Repeat the Step 7
The reference profile R_1 is matched with each cluster
one less distance segment is obtained using Euclidean distance
Again, this less distance cluster is matched with grid profile; finally, we obtain one less distance cluster or road segment using Euclidean distance.
Obtain the seed point R_2
Output
Initial seed points in road R_2
end

distance segment is obtained using Euclidean distance. Again, this less distance cluster is matched with R_1, finally, we obtain the one less distance cluster or road point R_2 using Euclidean distance. This R_2 is used for the further processing. The pseudo-code for seed point selection is given in Table 3.

4.2. *Measurement model for object tracking*

The innovative road extraction technique is home to two vital segments such as the PF module and the PLS module. The method employed to achieve the measurement data differs in each module and is tailored for various roles which each module has to play in the overall road extraction technique.

4.2.1. *Measurement for PF module*

Subsequent to the seed point choice, we trace the road employing the PF. The processing system the PF elegantly commences its functioning from an initial point on the road and subsequently, it sequentially moves to the next point on the road by employing certain synthetically defined time-step. The PF furnishes an effective way

to estimate (3) and (4) recursively by means of the Monte Carlo numerical approximation techniques. In this innovative technique, the filter evaluates the posterior density function with the help of a set of arbitrary samples and their matching weights (U_K^i, W_K^i) named particles. The posterior density is approximated by means of the following relation:

$$P(U_K|V_{1:K}) \approx \sum_{j=1}^{N} W_K^j \, \delta(U_K - U_K^i) \, . \tag{16}$$

When we are able to get sufficient samples from a PDF, the set of samples may be deployed to intimately characterize that distribution. Hence, by means of Eq. (16), we are able to create the samples U_K^i directly from the posterior density $P(U_K|V_{1:K})$, presuming equal weights $W_K^i = 1$. Nevertheless, in actual practice, the captioned posterior density does not make its presence every time. Hence, we are able to create samples only from certain other density function known as the *importance density function*.[12] Here, by appropriately weighing the sample set, we are able to approximate the pdf by utilizing the captioned equation. In an iterative method to the estimation issue, in the course of the Kth step, the set of particles is modernized in accordance with the particles in the prior particles. At the outset, for each $i = 1 : N$, a new particle is sampled from the importance density function as shown below:

Update samples:

$$U_K^i \sim q(U_K|U_{K-1}^i, V_K) \, . \tag{17}$$

Subsequently, the importance weights are estimated up to a normalizing constant as per the ensuing equation and by employing the matching importance weights from $(K-1)$th step

Update weights:

$$\tilde{W}^i_K = W^I_{K-1} \frac{P(V_K|U_K^i) P(U_K^i|U_{K-1}^i)}{q(U_K|U_{K-1}^i, V_K)} \, . \tag{18}$$

These weights are adapted by $W_K^i = \tilde{W}^i_K / \sum_{j=1}^{N} \tilde{W}^j_K$. The selection of importance density function $q(U_K|U_{K-1}^i, V_K)$ represents a significant challenge in the design of the PF. As far we are concerned, we employ the conventional prior, viz. $P(U_K|U_{K-1}^i)$, as the importance density function. By means of this selection, (12) and (13) are simplified as detailed below:

Update samples:

$$U_K^i \sim p(U_K|U_{K-1}^i) \, . \tag{19}$$

Update weights:

$$\tilde{W}^i_K = W_{K-1}^i \times p(V_K|U_K^i) \, . \tag{20}$$

At last, the updated particles function as prior for the subsequent state prior particles and this recursive function go on till the final state forecast and updating. This module generates N particles from R_2 and continues with the PF algorithm in accordance with (17)–(20). Quite different from any occlusion, an intersection or even remarkable change in the road direction the PF concludes the task of tracking. Hence, the PLS is competent to trace the road states in case of harsh occlusion caused in the road.

4.2.2. *Measurement model for multiple kernels PLS module*

With an eye on initializing the kernel PLS phase, the PF phase repositions the data on its previous victorious step of the current road segment onto the k-PLS phase. The PLS commences its task with a single road branch by employing the previous victorious state evaluation of the PF phase as its initial point. In the document, we regard the RT as a classification issue which marks the target (positive) and background (negative) feature variables with various values. To do the nonlinear task, kernel functions are introduced in PLS algorithm. Here, we combine multiple kernels (MKs) to develop a new hybrid kernel that improves the tracking performance of the system. By introducing the hybrid kernel, PLS can perform flexibility in the form of choice the road points.

In hybrid PLS, new hybridized kernel functions are taken and the RT function is performed based on this hybrid kernel functions. Let k_1 and k_2 be kernels over $\Xi \times \Xi, \Xi \subseteq R^d$. Then, three hybrid kernels are formulated based on the definition given in,[20]

- $k(x_i, x_j) = k_1(x_i, x_j) + k_2(x_i, x_j)$ is a kernel,
- $k(x_i, x_j) = \alpha * k_1(x_i, x_j)$ is a kernel, when $\alpha > 0$,
- $k(x_i, x_j) = k_1(x_i, x_j) * k_2(x_i, x_j)$ is a kernel,

In PLS model, we regard the RT as a classification issue which marks the target (positive) and background (negative) feature variables with various values. Within the PLS formulation, the variables in our RT process comprise two classes such as the feature vector and class label. In the ensuing section, we employ $U \in R^m$ to indicate the feature space for object portrayal and $V \in R$ to signify the class label space for an object. When the target object is identified by means of the PF phase which is deemed as the initial point, we get a positive sample u_1 by extorting a feature vector from the warped image indicated by the state parameter. In case additional positive samples are required for training, we create the virtual data by minimal perturbation and extort the matching feature vectors. With the intent to gather the negative samples, we arbitrarily draw samples from an annular region expressed by $\gamma < \|O_{\text{neg}} - O\| < \beta$ in which O represents the target location and O_{neg} characterizes the location of a negative sample. With the achieved road point, we

employ the PLS evaluation to decide an appearance model of the target object. The steps involved in object tracking based on k-PLS are explained follows:

(i) Applying first theorem

Step 1: At first we randomly initialize y

Step 2: To calculate the kernel-based score component x

$$x = k_{H'} y \,. \tag{21}$$

Step 3: Substitute the first theorems in Eq. (21), here k_1 is radial basis function and k_2 is the quadratic kernel. The first theorem to apply Eq. (21), we get,

$$x = (k_1(x_i, x_j) + k_2(x_i, x_j))y \,. \tag{22}$$

Step 4: After that to calculate the weight vector b_1 based on Eq. (22)

$$b_1 = V^T x \tag{23}$$

$$b_1 = V^T((k_1(x_i, x_j) + k_2(x_i, x_j))y) \,. \tag{24}$$

Step 5: Based on the above equation finally, we calculate $y = Vb_1$

$$y = V[V^T((k_1(x_i, x_j) + k_2(x_i, x_j))y)], \quad y \leftarrow y/\|y\| \,. \tag{25}$$

Step 6: Repeat Steps 2–6 until convergence

Deflate $(k_1 + k_2), V$ matrices: $(k_1 * k_2) \leftarrow (k_1 - xx^T k_1)(k_1 - xx^T k_1)^T + (k_2 - xx^T k_2)(k_2 - xx^T k_2)^T$

$$V \leftarrow V - xx^T V \,. \tag{26}$$

(ii) Applying the second theorem

When applying the second theorem to the PLS, at first, we randomly initialize y value. After that, we calculate the kernel-based score component x.

$$x = k_{H''} y \tag{27}$$

where

$k_{H''} \rightarrow$ Kernel, $k_{H''} = \alpha^* k_1(x_i, x_j)$.

After that, we substitute the kernel value (second theorem) to Eq. (27), we get,

$$x = (\alpha * k_1(x_i, x_j))y \,. \tag{28}$$

After calculating the score component, we calculate the weight vector b_1 based on the score component x.

$$b_1 = V^T x \,, \tag{29}$$

$$b_1 = V^T((\alpha^* k_1(x_i, x_j))y) \,. \tag{30}$$

Using above equation, we calculate y value

$$y = V b_1 \,,$$

$$y = V[V^T((\alpha^* k_1(x_i, x_j))y)], \quad y \leftarrow y/\|y\|. \tag{31}$$

Deflate $(\alpha, k_2), V$ matrices: $(\alpha, k_2) \leftarrow \alpha(k_1 - xx^T k_1)(k_1 - xx^T k_1)^T$

$$V \leftarrow V - xx^T V\,. \tag{32}$$

(iii) Applying the third theorem

In this section, we explain the third theorem. Here, we use the kernel are $k_{H''}$ which is $k_1(x_i, x_j)^* k_2(x_i, x_j)$. When we apply the kernel to the PLS, we obtain the output is obtained in Eq. (33).

$$x = (k_1(x_i, x_j)^* k_2(x_i, x_j))y\,. \tag{33}$$

Using Eq. (33), we calculate the weight vector b_1 based on Eq. (33)

$$b_1 = V^T x\,, \tag{34}$$

$$b_1 = V^T((\alpha^* k_1(x_i, x_j))y)\,. \tag{35}$$

The above equation is used to calculate the weight vector. Finally, we calculate the $y = V b_1$,

$$y = V[V^T((\alpha^* k_1(x_i, x_j))y)], \quad y \leftarrow y/\|y\|\,. \tag{36}$$

Deflate $(k_1 + k_2), V$ matrices:

$$(k_1 + k_2) \leftarrow (k_1 - xx^T k_1)(k_1 - xx^T k_1)^T * (k_2 - xx^T k_2)(k_2 - xx^T k_2)^T\,,$$

$$V \leftarrow V - xx^T V\,. \tag{37}$$

The weight vectors mirror the significance of each original feature variable for object portrayal and categorization. If each feature variable in the chosen feature space U represents a function of a pixel location in an object region, then the significance of this feature variable is linked to the discriminability between the target and the background classes at a specified location. Hence, we are able to employ weight to produce a saliency (importance) map, which illustrates the discriminative caliber of diverse locations in an object region. For instance, if each variable defines the intensity of one pixel and a feature vector signifies the band of pixel intensities in an object region, a subspace can be comprehended by the PLS assessment with certain positive and negative samples.

4.2.3. *Two-stage RT algorithm*

The main idea of our proposed approach is to track the road from satellite images using PF and multi-kernel particle least square analysis (MK-PLS) algorithms. At first, we calculate the initial seed point using K-means clustering algorithm. Once we calculate the seed point, based on the seed point PF algorithm tracking the road point from the satellite image. The PF component is responsible for tracking axis

Table 4. Pseudo-code for overall process of RT.

Input:
The parameter of PF algorithm
The parameter of the PLS algorithm
The parameter of satellite image
output:
Road segment
Assumption:
Input image S_{im}, initial leader point R_{in}, weight W, Probability value P_i, $W_K^i = 1$.
Start
Pick up the initial leader point
{
Randomly select one reference profile R_1 which is in the form of $n \times m$ matrix
Based on the R_1, create the grid and rearrange the image into a grid format.
}
Repeat
{
Apply the K-means algorithm to the grid image
Obtain the seed point R_2
}
for each next point selection apply PF
{
calculate the posterior density function using (16)
Calculate the weight of the point using (18)
Predict the next point using (19)
Update the next point using (20)
}
Repeat
If there is an obstacle in the road; stop the criteria
Then
{
Continues the tracking process using hybrid kernel-based PLS algorithm
}
for each next point selection
{
Get the input from the PF
Select the target (positive) and background (negative) value
Calculate the weight matrix
Apply the multiple to each point
Obtain the next point}
Repeat still road is segmented from the S_{im}.
Stop
Output:
Segmented road
end

coordinates of a road until it comes to severe obstacles or an intersection. If any obstacles arrive means the process is continued using the MK-PLS algorithms. The MKs are combined with PLS algorithm still road is tracked from the image which improves the tracking performance.

5. Result and Discussion

We now describe the result of experimentation using our proposed framework. The performance of the proposed method is verified using satellite images of size 512×512 each. The dataset (250 images) used here consists of five categories of satellite images, with 50 per category. This is split equally into two parts — one (125) used for training and another for testing. The performance of proposed techniques is compared with different state-of-the-art techniques. The proposed technique is performed in a windows machine having configurations Intel (R) Core i5 processor, 3.20 GHz, 4 GB RAM, and the operating system platform is Microsoft Window 7 Professional. We have used MATLAB latest version (7.12) for this proposed technique.

5.1. *Data set description and performance measures*

We have elegantly generated a database for the satellite image with 1-m/pixel resolution from *Wikimedia*. The quality of the image is dependent on the sensor employed in the climatic situations. For this experimentation, we used the five types of satellite images. The input image size is 1200×900 pixels. To assess the performance of the road extraction system in this work, we utilize the four evaluation measures such as accuracy, sensitivity, specificity, completeness and correctness.

Sensitivity: Sensitivity is the proportion of true positives that are correctly identified by a proposed method. It shows how good the test is at detecting a road.

$$\text{Sensitivity} = \frac{\text{TP}}{\text{TP} + \text{FN}} . \tag{38}$$

Specificity: Specificity is the proportion of the true negatives correctly identified by proposed method. It suggests how good the test is at identifying the normal (negative) condition.

$$\text{Specificity} = \frac{\text{TN}}{\text{TN} + \text{FP}} . \tag{39}$$

Accuracy: Accuracy is the proportion of true results, either true positive or true negative, in a population.

$$\text{Accuracy} = \frac{\text{TN} + \text{TP}}{\text{TN} + \text{FP} + \text{FN} + \text{FP}} . \tag{40}$$

Completeness: Completeness is defined as the percentage of the reference data which was detected during road extraction.

$$\text{Completness} = \frac{\text{length of matched reference}}{\text{length of reference}} . \tag{41}$$

Correctness: Correctness represents the percentage of the extracted road data which is correct

$$\text{Correctness} = \frac{\text{length of matched extraction}}{\text{length of extraction}} . \tag{42}$$

5.2. *Experimental results*

The basic idea of our research is to track the road based on the MK-PLS analysis with PF from the satellite images. To evaluate the performance of our proposed approach, we compare our results with different approaches. We have chosen five images to show in detail behavior of the proposed approach. In the five images, a sinuous but very homogeneous road is shown. The RT performance of proposed and previous approach with three images is presented. In our work, at first, we calculate the initial point of the road using K-means clustering algorithm. This initial point is used to further track the road accurately. Based on the clusters, the tracking process is started. Figure 2 shows the performance of the satellite image using different cluster values.

In our work, we use a different kernel with PLS. At first, we apply the PF to the initial point to obtain the tracking the road. If any obstacles are present in the road the PF stops the process. After that, the ending point itself the PLS start the process. The PLS address the poor generalization properties, so overcome this problem we utilize kernel with PLS algorithm. Further, improve the performance of the RT in our work we utilize the two types of kernels (quadratic kernel and radial basis

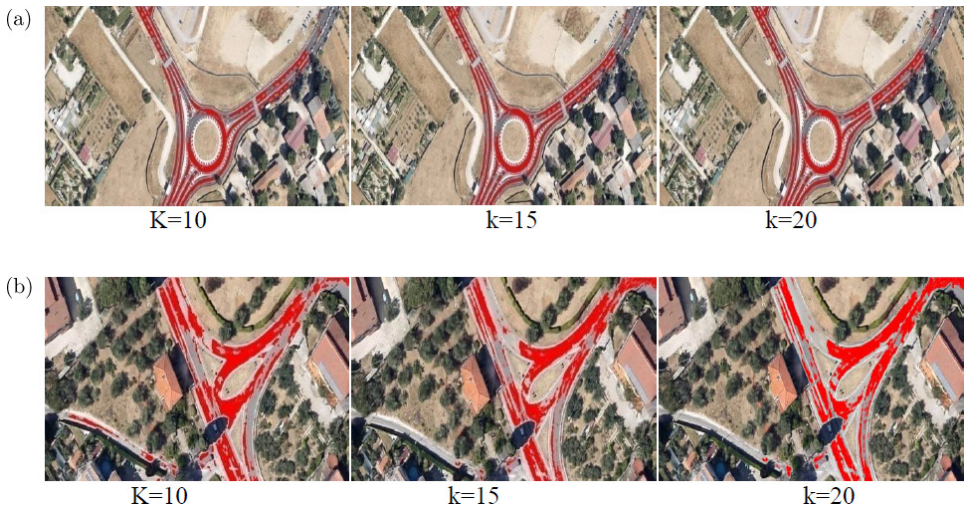

Fig. 2. Results obtained from proposed approach using PF+ MK-PLS for different cluster values (a) image 1 and (b) image 2.

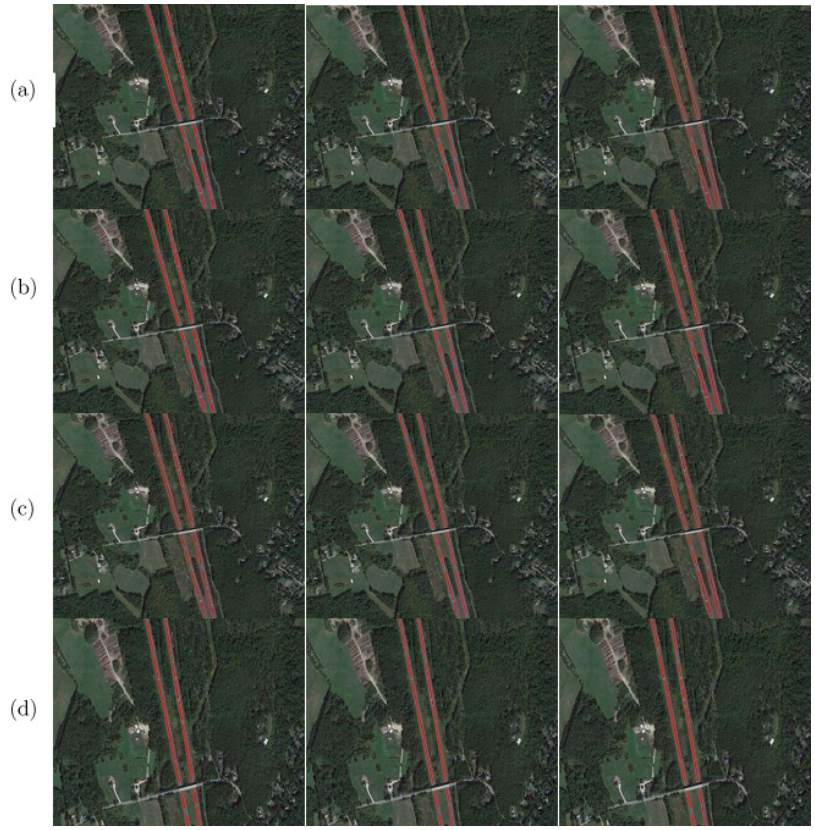

Fig. 3. (a) Results obtained from proposed approach using Theorem 1, (b) result obtained from using Theorem 2 and (c) result obtained from using Theorem 3 in image 1.

AQ: Please check edit.

function) with PLS. Finally, we obtain the road map from the satellite image without information losing. Figures 3–5 show the experimental result of RT using different approaches. In this experiment, we utilize the three types of the image; each image having three cluster values theses are shown in the corresponding image.

5.3. *Performance evaluation*

In this section, we provide the performance of the proposed approach using three types of theorems. Here, we employ five benchmark functions in our work which are explained in Eqs. 38–42. We choose these benchmark functions because they are being widely used by many researchers in the study of RT. The experimentation carried out five different types of satellite images to take our RT process. The result obtained by using three types of the theorem shown in Tables 5–9.

To evaluate the performance of our proposed approach, we compare our result with different theorems. Here, each theorem using the different kernels such as radial

Fig. 4. (a) Results obtained from proposed approach using Theorem 1, (b) result obtained from using Theorem 2 and (c) result obtained from using Theorem 3 in image 2.

AQ: Please check edit.

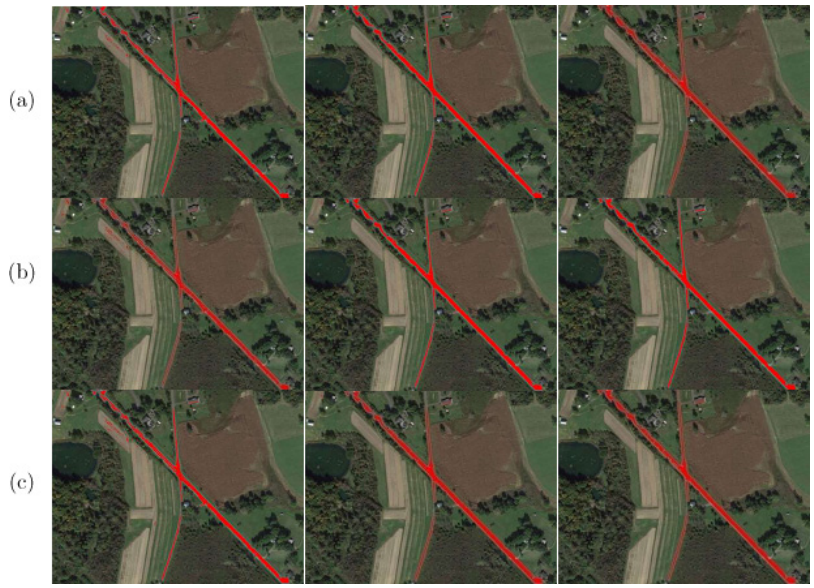

Fig. 5. (a) Results obtained from proposed approach using Theorem 1, (b) result obtained from using Theorem 2 and (c) result obtained from using Theorem 3 in image 3.

AQ: Please check edit.

Table 5. Performance comparison table for using different theorems in image 1.

Images	No. of clusters	Performance measures	Theorem 1	Theorem 2	Theorem 3
	10	Accuracy	98.0917	98.2237	98.1857
		Completeness	98.5769	98.7308	98.714
		Correctness	95.5989	95.7309	95.6929
		Sensitivity	22.8665	28.1938	26.6571
		Specificity	99.9997	100	100
	15	Accuracy	98.309	98.0832	98.106
		Completeness	98.8041	98.5786	98.5952
		Correctness	95.8162	95.5904	95.6132
		Sensitivity	31.6412	22.5131	23.4351
		Specificity	100	100	100
	20	Accuracy	98.2224	98.2151	98.2077
		Completeness	98.7099	98.7112	98.709
		Correctness	95.7304	95.7223	95.715
		Sensitivity	28.158	27.8455	27.5484
		Specificity	99.9996	100	100

Table 6. Performance comparison table for using different theorems in image 2.

Images	No. of clusters	Performance measures	Theorem 1	Theorem 2	Theorem 3
	10	Accuracy	98.2963	98.1778	98.1634
		Completeness	98.5526	98.4008	98.3936
		Correctness	96.3294	96.212	96.1975
		Sensitivity	16.813	11.0591	10.3543
		Specificity	100	99.9993	99.9993
	15	Accuracy	98.2698	98.3304	98.3152
		Completeness	98.5358	98.6218	98.6138
		Correctness	96.3029	96.3635	96.3483
		Sensitivity	15.5187	18.4789	17.7356
		Specificity	100	100	100
	20	Accuracy	98.1386	98.1799	98.1861
		Completeness	98.3735	98.44	98.4443
		Correctness	96.1717	96.213	96.2192
		Sensitivity	9.1113	11.1296	11.4308
		Specificity	100	100	100

Table 7. Performance comparison table for using different theorems in image 3.

Images	No. of clusters	Performance measures	Theorem 1	Theorem 2	Theorem 3
	10	Accuracy	97.5798	97.5815	97.4885
		Completeness	98.435	98.2766	98.2279
		Correctness	95.0932	95.0875	94.9905
		Sensitivity	40.228	37.4734	35.0028
		Specificity	99.8314	99.9413	99.9416
	15	Accuracy	97.9424	98.0003	98.037
		Completeness	98.6519	98.6849	98.6981
		Correctness	95.4428	95.5023	95.5393
		Sensitivity	46.2605	47.8901	48.9217
		Specificity	99.9714	99.9676	99.9652
	20	Accuracy	98.0305	97.991	97.9262
		Completeness	98.7396	98.7152	98.6933
		Correctness	95.5359	95.5004	95.4308
		Sensitivity	48.7498	47.8041	45.969
		Specificity	99.9652	99.9613	99.966

Table 8. Performance comparison table for using different theorems in image 4.

Images	No. of clusters	Performance measures	Theorem 1	Theorem 2	Theorem 3
	10	Accuracy	97.9424	98.0003	98.037
		Completeness	98.6519	98.6849	98.6981
		Correctness	95.4428	95.5023	95.5393
		Sensitivity	46.2605	47.8901	48.9217
		Specificity	97.9424	98.0003	98.037
	15	Accuracy	98.0917	98.2237	98.1857
		Completeness	98.5769	98.7308	98.714
		Correctness	95.5989	95.7309	95.6929
		Sensitivity	22.8665	28.1938	26.6571
		Specificity	100	100	100
	20	Accuracy	97.5798	97.5815	97.4885
		Completeness	98.435	98.2766	98.2279
		Correctness	95.0932	95.0875	94.9905
		Sensitivity	40.228	37.4734	35.0028
		Specificity	97.5798	97.5815	97.4885

Table 9. Performance comparison table for using different theorems in image 5.

Images	No. of clusters	Performance measures	Theorem 1	Theorem 2	Theorem 3
	10	Accuracy	98.1386	98.1799	98.1861
		Completeness	98.3735	98.44	98.4443
		Correctness	96.1717	96.213	96.2192
		Sensitivity	9.1113	11.1296	11.4308
		Specificity	100	100	100
	15	98.2224	98.2151	98.2077	98.2224
		98.7099	98.7112	98.709	98.7099
		95.7304	95.7223	95.715	95.7304
		28.158	27.8455	27.5484	28.158
		99.9996	100	100	99.9996
	20	Accuracy	97.9424	98.0003	98.037
		Completeness	98.6519	98.6849	98.6981
		Correctness	95.4428	95.5023	95.5393
		Sensitivity	46.2605	47.8901	48.9217
		Specificity	97.9424	98.0003	98.037

AQ: Please check.

basis function and quadratic kernel. From Tables 5–9, we obtain the average accuracy of 98.004% for Theorem 1, 98.024% for Theorem 2 and 98.087% for Theorem 3 for cluster size 10. In this approach, the kernel function is used to improve the performance of the proposed approach.

AQ: Please check edit.

5.4. *Comparative analysis*

To evaluate the performance of our proposed approach, we compare our results with our previous methods. Here, we compare our work with four approaches such as EKF+PF,[40] LEGION,[50] UKF+GHKF[45] and LEGION+GHKF.[46] Furthermore, these approaches characterize the local features of the road, based on the initial point, visual features and contrast. Therefore, we have chosen to compare the performance of our proposed algorithm against that of these ones. In Ref. 40, the author explained the road extraction from satellite image based on PF and EKF (PF+EKF). This method very well explains the RT, even though the deficiency of the algorithm is slow for PF module and it is more complex for urban areas. In Ref. 50, the author explained the LEGION-based automatic road extraction from a satellite image. This LEGION method is not very sensitive to particular parameters. In our first paper,[45] we extract the road from satellite image using UKF and GHKF. This method is efficient for road extraction even though it takes a lot of time. By reducing the process time and improving the extracted details, in our second paper, we introduced LEGION and GHKF-based road extraction from high-resolution satellite images.[46] To overcome the complexity present in the above methods, we further introduced the proposed method. From the result, one can observe that LEGION+GHKF[46] method and our

proposed one yield the best performance followed by EKF+PF,[40] UKF+GHKF[45] and LEGION.[50] This is because these methods very well describe the features of the satellite image. Compared to LEGION+GHKF[46] method our proposed method is slightly better[46] because of the use of hybrid kernel. To prove the effectiveness of the approach, we compare our proposed work with different measures such as accuracy, completeness and correctness.

AQ: Please approve edit.

Tables 10–14 shows the comparative analysis of proposed approach based on different measures. Table 10 shows the performance of proposed approach against existing approaches such as EKF+PF,[40] UKF+GHKF,[45] LEGION[50] and LEGION+GHKF[46] for image 1. In Table 6, when the cluster value is 20, we obtain the maximum accuracy of 98.4 for proposed approach which is 97.0 using EKF+PF,[40] 97.2 using UKF+GHKF,[45] 97.4 using LEGION[50] and 97.9 using LEGION+GHKF.[46] The performances in terms of completeness and correctness measures at the different clustering stages of proposed against existing approach also given in Table 10. When analyzing this measures, our proposed approach achieves the high completeness of 98.4 and high correctness of 95.8. Moreover, Table 11 shows the comparative analysis of proposed approach against existing work for image 2. From Table 11, we can view all the methods are more or equal accuracy value. In the method LEGION+GHKF[46] having the maximum accuracy of 98.5 which is slightly better than our proposed method. The higher completeness value is producing the better performance of the tracking process. The performance in terms of correctness measure at different clustering stages of proposed against existing approach also shown in Table 11.

Table 10. Comparative analysis of proposed approach based on different measures for image 1.

Measures	Accuracy			Completeness			Correctness		
Cluster size	10	15	20	10	15	20	10	15	20
EKF+PF[40]	97.5	97.6	97.0	97.7	98.0	97.5	95.0	95.1	95.3
LEGION[50]	98.1	98.1	97.4	98.7	98.8	98.7	95.7	95.7	95.7
UKF+GHKF[45]	98.2	98.2	97.2	1.0	1.0	0.76	95.6	95.6	95.3
GHKF+LEGION[46]	98.2	98.2	97.9	98.7	98.0	98.7	95.7	95.7	95.7
PF+MK-PLS	98.3	98.2	98.4	102.4	102.3	102.4	96.6	96.6	96.7

Table 11. Comparative analysis of proposed approach based on different measure for image 2.

Measures	Accuracy			Completeness			Correctness		
Cluster size	10	15	20	10	15	20	10	15	20
EKF+PF[40]	97.9	97.9	97.9	97.9	98.3	97.9	95.9	95.9	95.9
LEGION[50]	98.2	98.4	98.4	98.8	98.7	98.7	96.4	96.4	96.4
UKF+GHKF[45]	97.9	98.2	98.2	0.1	0.5	0.4	95.9	96.2	96.2
GHKF+LEGION[46]	98.5	98.4	98.4	98.9	98.8	98.7	96.5	96.4	96.4
PF+MK-PLS	98.3	98.5	98.3	102.2	102.4	102.3	97.2	97.3	97.2

Table 12. Comparative analysis of proposed approach based on different measures for image 3.

Measures	Accuracy			Completeness			Correctness		
Cluster size	10	15	20	10	15	20	10	15	20
EKF+PF[40]	96.5	96.2	96.6	97.5	96.4	97.8	93.9	93.7	94.0
LEGION[50]	97.3	97.5	97.5	98.1	98.4	98.4	95.6	94.5	95.6
UKF+GHKF[45]	98.1	97.0	98.1	2.8	2.1	2.8	94.8	95.1	95.1
GHKF+LEGION[46]	97.5	97.6	97.6	98.4	98.6	98.6	94.9	95.2	95.1
PF+MK-PLS	9.7	98.6	98.2	101.9	102.2	102.3	96.0	96.3	96.5

Similarly, performance in terms of accuracy, completeness and correctness measure at different clustering stages of our proposed framework for image 3 is shown in Table 12. In Table 12, our proposed work achieves the maximum accuracy of 98.6 which is 97.6 for using LEGION+GHKF,[46] 97.5 for using LEGION,[50] 97 for using UKF+GHKF[45] and 96.2 for using EKF+PF.[40] Similarly, we obtain the maximum completeness of 98.4 and correctness of 95.6. From Table 12, we clearly understand our proposed approach achieves the maximum accuracy, completeness, and correctness compared to the existing approaches. Moreover, Table 13 shows the performance of proposed approach against existing approaches such as EKF+PF,[40] UKF+GHKF,[45] LEGION[50] and LEGION+GHKF[46] for image 4. Here, when used cluster value is 15, we obtain the maximum accuracy of 91.4 which is high compared to EKF+PF,[40] UKF+GHKF,[45] LEGION[50] and LEGION+GHKF.[46] The methods

Table 13. Comparative analysis of proposed approach based on different measures for image 4.

Measures	Accuracy			Completeness			Correctness		
Cluster size	10	15	20	10	15	20	10	15	20
EKF+PF[40]	90.5	90.6	90.7	92.1	92.1	92.2	88.2	88.2	88.3
LEGION[50]	90.7	90.8	90.8	92.2	92.2	92.3	88.3	88.5	88.4
UKF+GHKF[45]	90.6	90.6	90.8	92.3	92.2	92.1	88.2	88.3	88.4
GHKF+LEGION[46]	90.9	90.9	91.1	92.1	92.2	92.3	88.6	88.5	88.8
PF+MK-PLS	91.3	91.4	91.5	91.8	91.8	91.9	88.8	88.8	88.9

Table 14. Comparative analysis of proposed approach based on different measures for image 5.

Measures	Accuracy			Completeness			Correctness		
Cluster size	10	15	20	10	15	20	10	15	20
EKF+PF[40]	85.9	85.2	85.4	88.7	88.1	88.4	81.8	80.9	81.3
LEGION[50]	86.5	85.6	85.7	88.7	88.1	88.5	81.5	81.1	81.3
UKF+GHKF[45]	85.6	85.2	85.4	88.8	88.2	88.5	82.4	81.5	81.6
GHKF+LEGION[46]	86.3	86.1	86.2	88.7	88.3	88.5	82.2	81.9	82.1
PF+MK-PLS	87.3	86.5	86.8	88.2	87.6	87.9	83.9	82.1	82.5

EKF+PF[40] are UKF+GHKF[45] obtain the most similar result using all the stages. The performance in terms of accuracy, completeness and correctness measures at different clustering stages of our proposed framework using image 5 is shown in Table 14. When using the cluster value is 20, we obtain the maximum accuracy of 86.8 which is very much high compared to the existing approach. From the entire above table, we clearly understand our proposed approach obtains the better results compared to other approaches.

6. Conclusion

We have developed an efficient algorithm based on a kernel hybridization for PLS analysis with PF as a RT approach for satellite images. At first, we calculate the initial leader point using K-means clustering algorithm which is useful for the further processing. After that, the PF traces a road still a stopping benchmark is satisfied. Subsequently, the hybrid kernel-based PLS algorithm performs the remaining LRT. To reduce the tracking drift, we using hybrid kernels such as the linear kernel and polynomial kernel with PLS approach. Compared with state-of-the-art tracking methods, the proposed algorithm achieves favorable performance with higher accuracy and lower tracking errors.

References

1. J. Subash and M. Kumar, Road tracking from high-resolution IRS and IKONOS images using unscented Kalman filtering, *Int. J. Electron. Signals Syst.* **1** (2014) 5–11.
2. S. Jyothi and D. K. Bhattacharya, A grid density based technique for finding clusters in satellite images, *Pattern Recognit. Lett.* **33** (2012) 589–604.
3. A. Baumgatner, S. Hinz and C. Wiedemann, Efficient methods and interfaces for road tracking, *Proc. Int. Arch. Photogramm. Remote Sens. ISPRS Commission III, Symp. 2002*, Vol. 34 part 3B, Graz, Austria, 9–13 September 2002, pp. 28–31.
4. M. Kass, A. Witkin and D. Terzopoulos, Snakes: Active contour models, *Proc. 1st Int. Conf. Computer Vision*, London, UK, (1987) pp. 259–268.
5. T. Kim, S. R. Park, M. G. Kim, S. Jung and K. O. Kim, Tracking road centerlines from high resolution remote sensing images by least squares correlation matching, *Photogramm. Eng. Remote Sens.* **70** (2004) 1417–1422.
6. J. Zhou, W. F. Bischof and T. Caelli, Road tracking in aerial images based on human–computer interaction and Bayesian filtering, *ISPRS J. Photogramm. Remote Sens.* **61** (2006) 108–124.
7. X. Hu, C. V. Tao and Y. Hu, Automatic road extraction from dense urban area by integrated processing of high resolution imagery and lidar data, *Proc. Int. Arch. Photogramm. Remote Sens. Spatial Inf. Sci. 20th ISPRS Congress, Technical Commission III*, Vol. 35, part B3, Istanbul, Turkey, 12–23 July 2004, pp. 320–324.
8. A. Gruen and H. Li, Semi-automatic linear feature extraction by dynamic programming and LSB-snakes, *Photogramm. Eng. Remote Sens.* **63** (1997) 985–995.
9. A. Baumgartner, C. Steger, H. Mayer, W. Eckstein and H. Ebner, Automatic road extraction based on multi-scale, grouping, and context, *Photogramm. Eng. Remote Sens.* **65** (1999) 777–785.

10. Y. Shao, B. Guo, X. Hu and L. Di, Application of a fast linear feature detector to road extraction from remotely sensed imagery, *IEEE J. Sel. Top. Appl. Earth Obs. Remote Sens.* **4** (2011) 626–631.
11. C. He, Z.-X. Liao, F. Yang, X.-P. Deng and M.-S. Liao, Road extraction from SAR imagery based on multiscale geometric analysis of detector responses, *IEEE J. Sel. Top. Appl. Earth Obs. Remote Sens.* **5** (2012), 1373–1382.
12. F. Benkouider, L. Hamami and A. Abdellaoui, Use of the neural net for road extraction from satellite images, application in the city of Laghouat, *Progress In Electromagnetic Research Symp. Proc.*, Marrakesh, Morocco (2011), pp. 1057–1061.
13. T. R. Mangala and S. G. Bhirud, A new automatic road extraction technique using gradient operation and skeletal ray formation, *Int. J. Comput. Appl.* **29** (2011) 17–25.
14. T. R. Mangala and S. G. Bhirud, Road network extraction from high resolution satellite images based on LSE–LBF model, *Int. J. Sci. Eng.* **2** (2011) 1–7.
15. G. Vosselman and J. D. Knecht, Road tracing by profile matching and Kalman filtering, *Processing Workshop Automatic Extraction Man-Made Objects Aerial Space Images* (Birkhäuser Basel, Monte Verità, 1995), pp. 265–274.
16. J. Zhou, W. F. Bischof and T. Caelli, Robust and efficient road tracking in aerial images, *Proc. Joint Workshop ISPRS and DAGM (CMRT) Object Extraction 3D City Models, Road Databases Traffic Monitoring — Concepts, Algorithms Evaluation*, Vienna, Austria (2005), pp. 35–40.
17. M. Bicego, S. Dalfini, G. Vernazza and V. Murino, Automatic road extraction from aerial images by probabilistic contour tracking, *Proc. ICIP*, Barcelona, Spain, 14–17 September 2003, pp. 585–588.
18. F. Tupin, H. Maitre, J. F. Mangin, J. M. Nicolas and E. Pechersky, Detection of linear features in SAR images: Application to road network extraction, *IEEE Trans. Geosci. Remote Sens.* **36** (1998) 434–453.
19. C. Zhu, W. Shi, M. Pesaresi, L. Liu, X. Chen and B. King, The recognition of road network from high-resolution satellite remotely sensed data using image morphological characteristics, *Int. J. Remote Sens.* **26** (2005) 5493–5508.
20. A. Katartzis, H. Sahli, V. Pizurica and J. Cornelis, A model-based approach to the automatic extraction of linear features from airborne images, *IEEE Trans. Geosci. Remote Sens.* **39** (2001) 2073–2079.
21. A. Baumgartner, C. Steger, C. Wiedemann, H. Mayer, W. Eckstein and H. Ebner, Update of roads in GIS from aerial imagery: Verification and multi-resolution extraction, *Proc. Int. Arch. Photogramm. Remote Sens.*, Vol. XXXI, Vienna, Austrian12–18 July 1996, pp. 53–58.
22. O. Tuncer, Fully automatic road network extraction from satellite images, *Proc. Recent Advances in Space Technologies*, Piscataway, NJ, 14–16 June 2007, pp. 708–714.
23. C. Steger, An unbiased detector of curvilinear structures, *IEEE Trans. Pattern Anal. Mach. Intell.* **20** (1998) 113–125.
24. M. Amo, F. Martinez and M. Torre, Road extraction from aerial images using a region competition algorithm, *IEEE Trans. Image Process.* **15** (2006) 1192–1201.
25. D. Geman and B. Jedynak, An active testing model for tracking roads in satellite images, *IEEE Trans. Pattern Anal. Mach. Intell.* **18** (1996) 1–14.
26. P. Gamba, F. Dell'Acqua and G. Lisini, Improving urban road extraction in high-resolution images exploiting directional filtering, perceptual grouping, and simple topological concepts, *IEEE Geosci. Remote Sens. Lett.* **3** (2006) 387–391.

27. M. Barzohar and D. B. Cooper, Automatic finding of main roads in aerial images by using geometric-stochastic models and estimation, *IEEE Trans. Pattern Anal. Mach. Intell.* **18** (1996) 707–721.
28. A. Doucet, S. Godsill and C. Andrieu, On sequential Monte Carlo sampling methods for Bayesian filtering, *Stat. Comput.* **10** (2000) 197–208.
29. M. Isard and A. Blake, Condensation — conditional density propagation for visual tracking, *Int. J. Comput. Vis.* **29** (1998) 5–28.
30. N. Gordon, D. Salmond and C. Ewing, Bayesian state estimation for tracking and guidance using the bootstrap filter, *J. Guid. Control Dyn.* **18** (1995) 1434–1443.
31. N. Gordon, M. S. Arulampalam, S. Maskell and T. Clapp, A tutorial on particle filters for online nonlinear/non-Gaussian Bayesian tracking, *IEEE Trans. Signal Process* **50** (2002) 174–188.
32. K. Nummiaro, E. Koller-Meier and L. Van Gool, Object tracking with an adaptive color-based particle filter, *Image Vis. Comput.* **21** (2002) 99–111.
33. P. N. Anil and Dr. S. Natarajan, Automatic road extraction from high resolution imagery based on statistical region merging and skeletonisation, *Int. J. Eng. Sci. Technol.* **2** (2010) 165–171.
34. J. Shen, X. Lin, Y. Shi and C. Wong, Knowledge-based road extraction from high resolution remotely sensed imagery, *Proc. Congress. Image Signal Process.* Vol. 4, Sanya, China, 27–30 May 2008, pp. 608–612.
35. D. Guo, A. Weeks and H. Klee, Robust approach for suburban road segmentation in high-resolution aerial images, *Int. J. Remote Sens.* **28** (2007) 307–318.
36. I. Laptev, H. Mayer, T. Lindeberg, W. Eckstein, C. Steger and A. Baumgartner, Automatic extraction of roads from aerial images based on scale space and snakes, *Mach. Vis. Appl.* **12** (2000) 23–31.
37. R. Marikhu, M. Dailey, S. Makhanov and K. Honda, A family of quadratic snakes for road extraction, *Computer Vision — ACCV 2007*, eds. Y. Yagi, S. B. Kang, I. S. Kweon and H. Zha (Springer, Berlin, 2007), pp. 85–94.
38. M. Song and D. Civco, Road extraction using SVM and image segmentation, *Photogramm. Eng. Remote Sens.* **70** (2004) 1365–1371.
39. M. Negri, P. Gamba, G. Lisini and F. Tupin, Junction-aware extraction and regularization of urban road networks in high-resolution SAR images, *IEEE Trans. Geosci. Remote Sens.* **44** (2006) 2962–2971.
40. S. Movaghati and A. Moghaddamjoo, Road extraction from satellite images using particle filtering and extended Kalman filtering, *IEEE Trans. Geosci. Remote Sens.* **48** (2010) 2807–2817.
41. A. P. Dal Poz, R. A. B. Gallis and J. F. C. da Silva, Three-dimensional semiautomatic road extraction from a high-resolution aerial image by dynamic-programming optimization in the object space, *IEEE Geosci. Remote Sens. Lett.* **7** (2010) 796–800.
42. J. Hu, A. Razdan, J. C. Femiani, M. Cui and P. Wonka, Road network extraction and intersection detection from aerial images by tracking road footprints, *IEEE Trans. Geosci. Remote Sens.* **45** (2007) 4144–4157.
43. A. P. Dal Poz, R. A. B. Gallis, J. F. C. da Silva and É. F. O. Martins, Object-space road extraction in rural areas using stereoscopic aerial images, *IEEE Geosci. Remote Sens. Lett.* **9** (2012) 654–658.
44. Z. Miao, W. Shi, H. Zhang and X. Wang, Road centerline extraction from high-resolution imagery based on shape features and multivariate adaptive regression splines, *IEEE Geosci. Remote Sens. Lett.* **10** (2013) 583–587.

45. K. M. Kumar and R. Kanthavel, Road extraction from satellite images using unscented Kalman filter and Gauss–Hermite Kalman filter, *Int. Rev. Comput. Softw.* **8** (2013) 2102–2112.
46. K. M. Kumar, R. Kanthavel and A. Velayudham, Automatic road network extraction through S-LEGION and GHKF using high resolution satellite images, *Inf., Int. Interdiscip. J.* **17** (2014) 4589–4598.
47. N. J. Gordon *et al.*, A novel approach for non-linear/non-Bayesian state estimation, *IEEE Proc. F* **140** (1993) 107–113.
48. X. Jin and C. H. Davis, An integrated system for automatic road mapping from high-resolution multi-spectral satellite imagery by information fusion, *Inf. Fusion* **6** (2005) 257–273.
49. R. Rosipal and N. Kramer, Overview and recent advances in partial least squares, *Latent Structures Feature Selection* (Springer-Verlag, New York, 2006), pp. 34–51.
50. J. Yuan, D. Wang, B. Wu, L. Yan and R. Li, LEGION-based automatic road extraction from satellite imagery, *IEEE Trans. Geosci. Remote Sens.* **49** (2011) 4528–4538.